INS/GPS Integration Architecture Performance Comparisons

George T. Schmidt
Massachusetts Institute of Technology
10 Goffe Road
Lexington, MA 02421
USA

Richard E. Phillips
Charles Stark Draper Laboratory
555 Technology Square
Cambridge, MA 02139
USA

ABSTRACT

Performance comparisons between the three major INS/GPS system architectures for various mission scenarios will be presented in order to understand the benefits of each. The loosely coupled and tightly coupled systems will be compared in several scenarios including aircraft flying against jammers and a helicopter flying a scout mission. The tightly coupled and deep integration architectures will be compared for several jamming scenarios including that of a precision guided munition.

1.0 INTRODUCTION

In Reference 1, INS/GPS integration architectures defined as loosely coupled, tightly coupled, and deeply integrated configurations were described. The advantages and disadvantages of each level of integration were listed. Examples of current and future systems were cited. In this paper, performance comparisons between the three major INS/GPS system architectures for various mission scenarios will be presented in order to understand the benefits of each. The loosely coupled and tightly coupled systems will be compared in several scenarios including aircraft flying against jammers and a helicopter flying a scout mission. The tightly coupled and deeply integrated architectures will be compared for several jamming scenarios including that of a precision guided munition.

2.0 LOOSELY COUPLED VS. TIGHTLY COUPLED PERFORMANCE COMPARISON

This section shows the jamming-related performance of loosely coupled and tightly coupled INS/GPS navigation systems in several hypothetical situations. In addition to comparing navigation architectures, the performance of inertial systems of varying quality was evaluated. The analysis considered only the performance of the combined INS/GPS solution and is thus appropriate to either of the loosely coupled architectures as they share the same INS/GPS solution. This particular example of an INS/GPS loosely coupled system has been the subject of numerous published studies [e.g., Ref. 2]. The tightly coupled system did not necessarily correspond to any particular existing system.

Several jamming scenarios were considered. The first scenario was designed to simply show the behavior of INS/GPS systems when GPS satellites are lost and reacquired one at a time. That is, there will be four satellites in track, then three, two, one, and finally zero. Then they were reacquired one at a time. For one of the scenarios, the navigation system was augmented with a Doppler ground speed measuring device.

2.1 Loosely Coupled System Definition

The loosely coupled GPS system consisted of a GPS receiver, an inertial navigation system, and an integration filter. The PVA solution from a typical receiver like the MAGR was used as the input to the INS/GPS

integration Kalman filter. In order to avoid the problem of dealing with correlated measurements, the integration filter only used the position from the PVA solution, and this only once every 10 s and only if the Expected Horizontal Error (EHE), a receiver output and measure of horizontal navigation quality, was less than 100 m. The receiver did not compute a solution if there were fewer than four satellites in track. The state elements for the GPS receiver are shown in Table 1.

Table 1: State Elements for the Unaided GPS Receiver.

State Element	Components
Position	3
Velocity	3
Acceleration	3
User clock bias	1
User clock drift	1
Altimeter bias	1
Total	12

Since the GPS receiver solution is the result of a (Kalman) filter, the velocity is correlated with the position, and both position and velocity are correlated in time. Process noise, which allows the filter to track changing acceleration, also decorrelates the output. The process noise is of such a magnitude that position solutions separated by 10-s intervals are not significantly correlated. The state elements of the integration filter that processes these measurements is shown in Table 2.

Table 2: State Elements for the Loosely Coupled Integration Filter.

Error State Element	Components
Position	3
Velocity	3
Misalignment	3
Gyro drift	3
Gyro scale factor	3
Accel. bias	3
Accel. scale factor	3
Altimeter bias	1
Total	22

Most Kalman filters are suboptimal estimators. Some are less near optimal than others. The cascaded filter architecture of loosely coupled systems is certainly far from optimal. These systems are particularly sensitive to the procedure known as "tuning," in which the process noise is added and measurements are down-weighted or omitted. A considerable effort went into tuning the loosely coupled INS/GPS system such that it could be compared fairly with the tightly coupled systems.

2.2 Tightly Coupled System Definition

The tightly coupled system consists of a receiver, inertial instruments, and an integration filter. The integration filter accepts measurements of pseudo-range and pseudo-range rate from each satellite at a 1-Hz rate. The filter state is extrapolated forward in time using inertial measurements and a model for the earth's gravity field. The state elements for this most straightforward approach are shown in Table 3. These same states appear in the cascaded filters of the loosely coupled system.

Table 3: State Elements for the Tightly Coupled Integration Filter.

Error State Element	Components
Position	3
Velocity	3
User clock bias	1
User clock drift	1
Misalignment	3
Gyro drift	3
Gyro scale factor	3
Accel. bias	3
Accel. scale factor	3
Altimeter bias	1
Total	24

2.3 Initial Errors, Modeling Errors, and Instrument Errors

These error sources influence the performance of the navigation system, some more than others. The initial errors in position, velocity, and misalignment in fact have very little effect on the performance of the system as long as it operates for a significant time. They are set to levels that are consistent with some kind of ground calibration and alignment mode, but are poor enough to show improvement as in-flight alignment progresses - - with either system architecture. Other errors can have significant effect on navigation system performance. Those errors that are independent of INS quality are given in Table 4. The Markov processes in this table are characterized by two numbers, a standard deviation, and a distance constant.

Table 4: Error Values for INS Independent Models.

Bias Errors	Modeled Value (1σ)	No. Components
Initial position	16 m (vertical)	1
	600 m (horizontal)	2
Initial velocity	0.3 m/s	3
GPS user clock		
Initial offset	5000 ms	3
Initial drift	10^{-2} ppm	
g-sensitive drift	10^{-3} ppm/g	
GPS pseudo-range	3.0 m	4
GPS range rate	0.003 m/s	4
Gravity (Markov)	35 µg/37 km	3
Barometer (Markov)	150 m/460 km	1
Noise errors		
GPS pseudo-range	from receiver tracking	4
GPS range rate	loop simulation	4
Barometer	3 m	1

The performance of four different IMU qualities were analyzed. The four IMUs were characterized by their navigation error after 1 h of unaided (inertial-only) operation. The error characteristics of actual inertial instruments whose performance was close to 10, 1, 0.5 and 0.2 nmi/h were scaled proportionally to yield those exact values.

The error values for each of these hypothetical instruments are shown in Table 5.

Table 5: IMU Error Sources.

	IMU Quality (All errors except random walk are 1σ biases)			
Error Source	**10 nmi/h**	**1.0 nmi/h**	**0.5 nmi/h**	**0.2 nmi/h**
Accel. bias	223 µg	37 µg	19 µg	4.2 µg
Accel. scale factor	223 ppm	179 ppm	90 ppm	21 ppm
Input axis misalign.	22 arcsec	3 arcsec	1.5 arcsec	0.4 arcsec
Random walk	56 µg/√Hz	15 µg/√Hz	7.5 µg/√Hz	4.2 µg/√Hz
Gyro bias	0.11 deg/h	0.0045 deg/h	0.0022 deg/h	0.00084 deg/h
Gyro scale factor	112 ppm	7.5 ppm	3.5 ppm	1.67 ppm
Input axis misalign.	22 arcsec	2.2 arcsec	1.1 arcsec	0.4 arcsec
Random walk	4.7 deg/h/√Hz	0.13 deg/h/√Hz	0.066 deg/h/√Hz	0.03 deg/h/√Hz

Initial misalignment error was derived from "gyrocompassing" each of the inertial units so it is instrument-dependent. Its values are not critical for the analysis because improvements in alignment due to in-flight maneuvers soon dominate the navigation results.

2.5   GPS Receiver Bandwidth, Loss of Lock and Reacquisition

For the loosely coupled receiver, the noise bandwidths of the code and carrier loop are fixed. The carrier was a third-order loop with bandwidth of 5.83 Hz. The code loop band is first order, but is aided by either the carrier loop if the carrier loop is in lock or by the INS if the carrier loop is not in lock. During carrier loop aiding, the code loop bandwidth is 1.5 Hz. During inertial aiding, the bandwidth is 0.5 Hz.

The bandwidths for the tightly coupled receiver were set appropriate to the quality of inertial instruments. These bandwidths are determined by the requirement that the loops stay in lock for a 10-g/s jerk, which lasts for 0.6 s. (The carrier tracking bandwidth was actually set for this study by requiring that the phase error be less than 90 deg for a 6-g acceleration step. This is a slightly more stringent requirement, but is easier to analyze.) The next several paragraphs present the method used for setting the tracking loop bandwidths. We took maximum advantage of knowing the inertial instrument performance. Closely tuning the tracking loops to the inertial performance in this way may not always be practical for actual receivers.

The phase error in a third-order loop following an acceleration step is shown in the following equation. (Note that distance has been converted to phase error in degrees using the code length of 300 m.)

$$\Delta\Phi = \frac{R}{\omega_0^2}\left[e^{-\omega_0 t} + \frac{e^{-\omega_0 t 2}}{\sqrt{3}}\left(\sin \omega_0 t \frac{\sqrt{3}}{2} - \sqrt{3}\cos\omega_0 t \frac{\sqrt{3}}{2}\right)\right]$$

where: R is the step magnitude (deg/s^2)

ω_0 is the filter natural frequency (rad/s)

$\Delta\Phi$ is the phase error in degrees

The natural frequency should be selected to keep the peak phase error less than 90 deg. The graph in Figure 1 shows the response, $\Delta\Phi$, for a natural frequency of 17.67 rad/s, the maximum error is 90 deg.
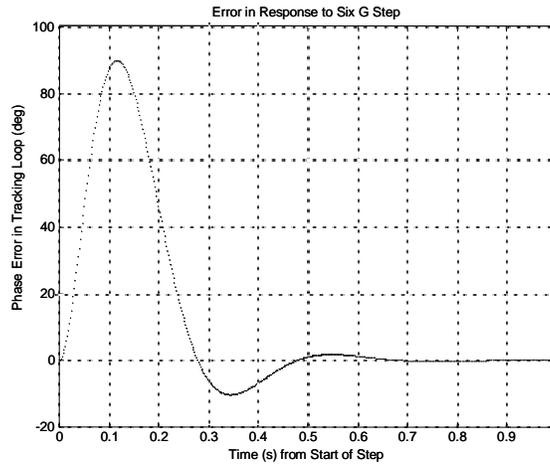
Figure 1: Error in third-order loop response to a 6-g step in acceleration.

With inertial aiding, the tracking loop will not be affected by the full magnitude of the step in acceleration. Only a residual part of the acceleration step due to imperfect inertial instruments will affect the tracking loop. The error, $\Delta\Phi$, is proportional to the step magnitude and inversely proportional to the square of the natural frequency. To maintain a 90-deg peak error, the natural frequency can be scaled by the square root of the ratio of aided to unaided step magnitude.

$$\omega_{0,aided} = \sqrt{\frac{R_{aided}}{R_{unaided}}}\,\omega_{0,unaided}$$

(2.1)

The residual error (post-calibration) accelerometer scale factor and IMU misalignment cause a residual acceleration step to be seen by the tracking loop. Lag in the inertial aiding would also add to the acceleration seen by the tracking loop. This lag was assumed to be negligible in this tightly coupled situation.

The residual acceleration seen by the tracking loop due to scale factor error is shown below.

$$\delta a_{sf} = \begin{bmatrix} sf_1 & 0 & 0 \\ 0 & sf_2 & 0 \\ 0 & 0 & sf_3 \end{bmatrix} a$$

IMU misalignment causes acceleration to be rotated incorrectly. The error in acceleration due to misalignment is shown below.

$$\delta a_{mis} = \begin{bmatrix} 0 & -\delta\theta_3 & \delta\theta_2 \\ \delta\theta_3 & 0 & -\delta\theta_1 \\ -\delta\theta_2 & \delta\theta_1 & 0 \end{bmatrix} a$$

The net error caused by scale factor and misalignment due to a unit acceleration step is thus:

$$\delta a = \delta a_{sf} + \delta a_{mis}$$

$$\delta a = \begin{bmatrix} 1 & 0 & 0 & 0 & -1 & 1 \\ 0 & 1 & 0 & 1 & 0 & -1 \\ 0 & 0 & 1 & -1 & 1 & 0 \end{bmatrix} \begin{bmatrix} sf_1 \\ sf_2 \\ sf_3 \\ \delta\theta_1 \\ \delta\theta_2 \\ \delta\theta_3 \end{bmatrix}$$

The covariance of residual acceleration error due to a unit acceleration step is shown below.

$$\langle \delta a \delta a^T \rangle = \begin{bmatrix} 1 & 0 & 0 & 0 & -1 & 1 \\ 0 & 1 & 0 & 1 & 0 & -1 \\ 0 & 0 & 1 & -1 & 1 & 0 \end{bmatrix} \begin{bmatrix} \sigma_{sf}^2 & c_{sf-mis} \\ c_{sf-mis} & \sigma_{mis}^2 \end{bmatrix} \begin{bmatrix} 1 & 0 & 0 \\ 0 & 1 & 0 \\ 0 & 0 & 1 \\ 0 & 1 & -1 \\ -1 & 0 & 1 \\ 1 & -1 & 0 \end{bmatrix}$$

The quantities σ_{sf}, and σ_{mis} are the scale factor and misalignment standard deviations. The quantity c_{sf-mis} is the covariance of these two quantities. This scale factor/misalignment matrix (the middle factor on the right) was taken from a covariance analysis after the aircraft had performed in-flight calibration maneuvers. If the scale factor is expressed as a fraction and the misalignment is in radians, the acceleration variance (on the left) will be the variance in acceleration seen by the tracking loop for a unit acceleration step. The radius of the sphere that enclosed 90% of these acceleration errors was taken to be the acceleration magnitude to which the tracking loops were tuned. Although a 90% level may not seem very robust, it should be remembered that tracking loop errors greater than 90 deg do not necessarily cause loss of lock.

For the four qualities of IMU studied, the radius of the acceleration sphere and the corresponding bandwidths are shown in Table 6. The error due to a unit acceleration step is given in parts per million.

**Table 6: The Residual Acceleration Error and Corresponding Bandwidth
for the Carrier Tracking Loop for Four IMU Qualities.**

IMU	Residual Error (90%) Due to Scale Factor and Misalignment (ppm)	Acceleration Seen by Tracking Loop Due to 6-g Acceleration Step	Required Carrier Tracking Loop Bandwidth
No inertial aiding	Not applicable	6 g	18 rad/s
10 nmi/h	1880	0.011 g	0.77
1 nmi/h	431	0.0026 g	0.37
0.5 nmi/h	311	0.0019 g	0.32
0.2 nmi/h	225	0.0014 g	0.27

The quantity in the second column is the radius of the sphere that encloses 90% of the errors. The quantities in the third column are that error times the 6-g acceleration step, and the quantities in the third column are the required bandwidth as determined by Eq. 2.1. For example, the bandwidth for the 10-nmi/h system was computed as shown below.

$$\omega_{0,aided} = \sqrt{\frac{0.011\,g}{6\,g}}\, 18\,rad/s = 0.77\,rad/s$$

For the purposes of the analysis, it was declared that the receiver had lost lock if the carrier phase error exceeded 90 deg or if the signal-to-noise ratio dropped below 19 dB. Loss of lock for the code phase was declared if the tracking error was greater then 1/2 chip (50 ns) or if the signal-to-noise ratio dropped below 18 dB. Conversely, reacquisition was dependent on achieving a signal-to-noise ratio of at least 21 dB for the code and 22 dB for the carrier for a required amount of time. The required time depends on the uncertainty in the range and range rate to each satellite and the rate at which each code phase and frequency combination could be searched.

At the given signal level, a 20-ms integration period should be adequate for accumulating signal energy. The size of the phase shift between 20-ms search intervals was 36 deg corresponding to 30 m. The size of the frequency bandwidth was 50 Hz corresponding to 10 m/s. The approximate time required to search over this position-frequency space (±σ) is given below.

$$\Delta T = 0.020 \left[\frac{2\,\sigma_{rng}}{30} \right] \times \left[\frac{2\,\sigma_{rng-rate}}{10} \right]$$

Some additional time must be added to allow for receiver moding. That is, the search process must be halted, and the receiver tracking loops cycled several times with an adequate signal-to-noise /jammer ratio.

2.6   Navigation Performance for Four Missions

Four missions were studied. The purpose of each of these mission scenarios was to observe the effects of jamming on loosely and tightly coupled INS/GPS systems and to observe the effect of IMU quality on tightly coupled systems. For the first scenario, the loss of lock and reacquisition for each of four satellites was spaced out so that the behavior of the navigation solution could be observed for extended periods of time between each loss. The other missions consisted of: 1) an aircraft flying past a jammer so that it loses lock then reacquires satellites as the jammer recedes into the distance, 2) an aircraft approaching a jammer head on, and 3) a helicopter operating in the vicinity of a jammer.

2.6.1   Sequential Outage

In this scenario, the loss of lock on satellite carrier and code phase was forced at 3-min intervals. Loss of code lock began after the fourth carrier tracking loop lost lock. Thus, the sequence began with loss of lock on a single carrier signal and ended with the loss of lock of the fourth code loop. Two variations in the study were considered at this point. In one of these, the signals were reacquired in inverse order after a total outage of 20 min. In the other variation, the mission was continued for 84 min using inertial measurements without the aid of GPS.

The behavior of the horizontal velocity error for the loosely and tightly coupled 1 nmi/h systems is shown in Figures 2 and 3.
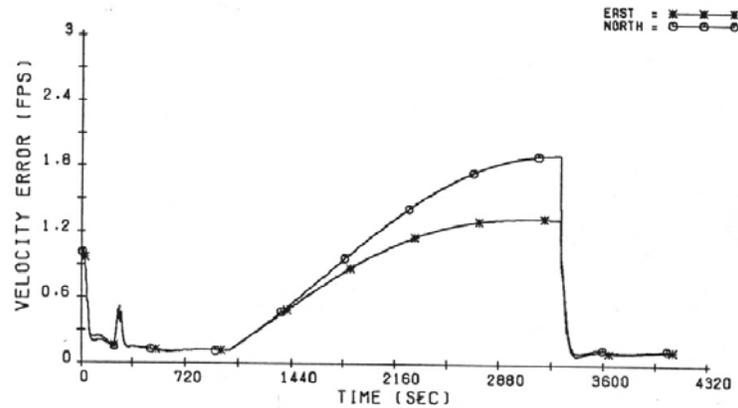
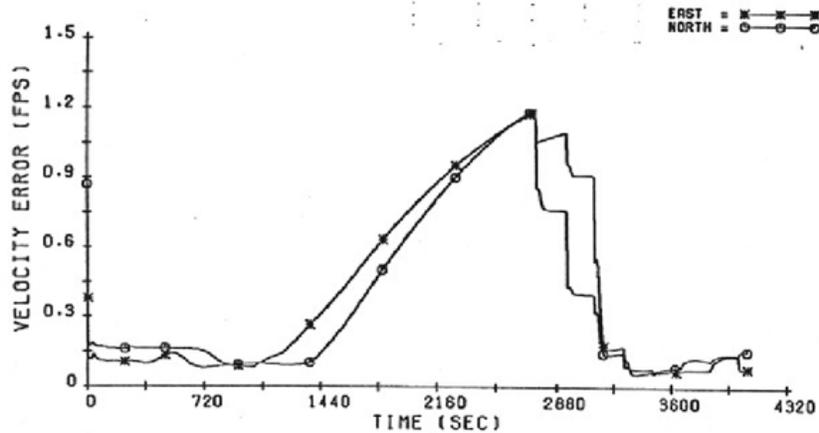**Figure 2: Horizontal velocity error for the loosely coupled navigation systems.**

Figure 3: Horizontal velocity error for the tightly coupled navigation systems.

The first loss of carrier tracking occurs at 360 s. The first loss of code at 1020 s. One feature of this loosely coupled system is that it does not form a navigation solution if fewer than four satellites are in lock. Thus, the immediate rise in velocity error begins at this point in the bottom graph (loosely coupled system). In contrast, the increase in velocity error for the tightly coupled system is somewhat delayed. The sequence of code reacquisition begins at 2760 s. Since the tightly coupled system makes immediate use of the first code measurement, the step improvement in velocity is seen at that time. The correlations between position and velocity in the Kalman filter cause the decrease in velocity error, even though it is a range measurement that has been made. Each successive code loop reacquisition causes a step improvement in the velocity accuracy. In contrast, the loosely coupled system does not get the benefit of the recently reacquired code phase until four satellites are in lock. At this point (in the lower graph), the improvement in velocity accuracy is recognized easily.

With four satellites in lock, the loosely coupled system yields perfectly acceptable navigation performance. The response to jamming the tightly coupled system is somewhat better. The maximum horizontal position error for each system studied is shown in Figure 4.
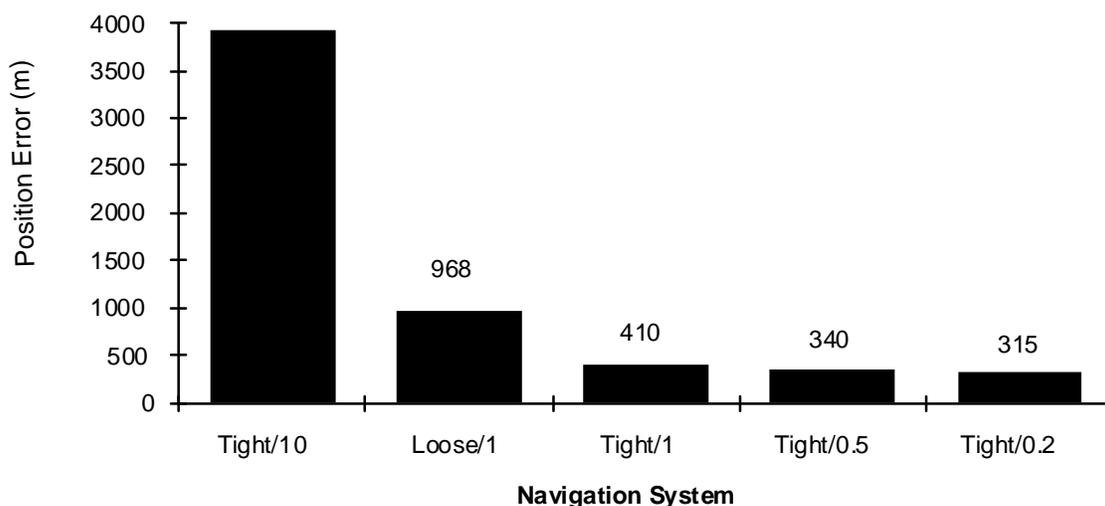
Figure 4: Horizontal position errors at time of reacquisition.

If the navigation system is denied, GPS measurements for 84 min, the horizontal position errors grow to the levels shown in Figure 5.
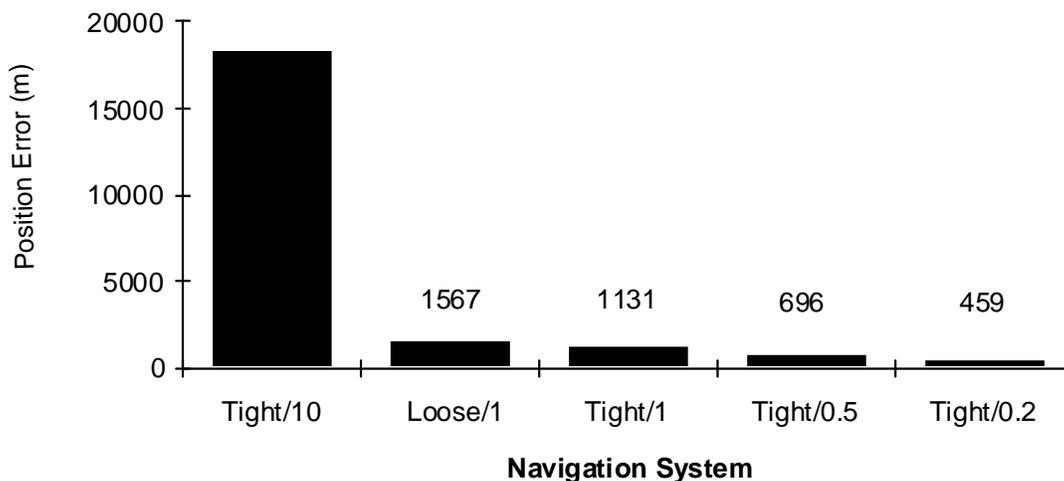

Figure 5: Horizontal position errors 1 Schuler period after loss of last satellite.

In addition to the obvious correlation of navigation error to IMU quality, we can make the following general observations about these results. The tightly coupled 1.0-nmi/h system does perform better than the loosely coupled system. This is due to two factors: 1) the tightly coupled system makes use of measurements even when fewer than four satellites are in lock, and 2) the calibration of the inertial instruments is somewhat better with the tightly coupled system. This performance difference diminishes with time. A very long time after the last GPS measurement, the performance of the tightly coupled and loosely coupled systems would be identical -- that of a 1-nmi/h system. The performance of the 1.0-nmi/h system is about 10 times better than that of the

10.0-nmi/h system at the end of the 20-min blackout interval. However, at the end of 84 min, the 1.0-nmi/h system has only drifted to a 1131 m error. The 10-nmi/h system has drifted to close to 18000 m. This simply reflects the fact that the major source of error for the 10-nmi/h system is uncalibratable random errors.

2.6.2 Jammer Flyby

For this scenario, an aircraft flies by a jammer, thus losing and regaining lock in a somewhat more realistic fashion. A jammer was placed on the ground near the midpoint of the trajectory to cause an approximate 20-min outage. In contrast to the previous situation in which the period of the outage was specified, in this scenario, the actual loss of lock will be determined by the signal-to-noise ratio for each satellite. Reacquisition will be determined by the growing uncertainty in range and range rate to each satellite. The period of outage will also be a function of the bandwidth of the carrier tracking loops for each of the receivers. We will, again, observe position and velocity error growth as GPS measurements are lost.

Table 7 shows the number of range intervals to be searched for each satellite at the time the signal-to-noise threshold rose above 21 dB. In no case did the error growth in velocity cause the range rate uncertainty to any satellite to be greater than 10 m/s (one Doppler shift interval).

Table 7: Search for Range Phase as a Function of IMU Quality.

| Navigation System | Range (Code Phase) Intervals to be Searched | | | | | | |
| | Satellite Identification | | | | | | |
	3	11	12	15	17	18	21
Tightly coupled 10 nmi/h	73	64	70	42	82	70	43
Loosely coupled 1.0 nmi/h	8	8	8	6	9	8	6
Tightly coupled 1.0 nmi/h	7	6	6	5	7	6	5
Tightly coupled 0.5 nmi/h	6	6	6	5	6	6	5
Tightly coupled 0.2 nmi/h	6	5	6	5	6	5	5

For a search time of 20 ms/chip (code phase interval), the better IMUs hold the search time to 0.2 s. The 10-nmi/h inertial system holds the search time to about 0.8 to 1.6 s. These numbers only reflect the error growth in position (and velocity) uncertainty and assume that the entire 1σ search area must be searched before lock on is achieved. Sometimes the signal will be found sooner, and of course, 32% of the time, it will be outside the 1σ bounds and require a longer search. Unfortunately, these results cannot be generalized. The placement of the jammer, its signal strength, the antenna orientation, and gain pattern are unique to the scenario and can only be considered typical.

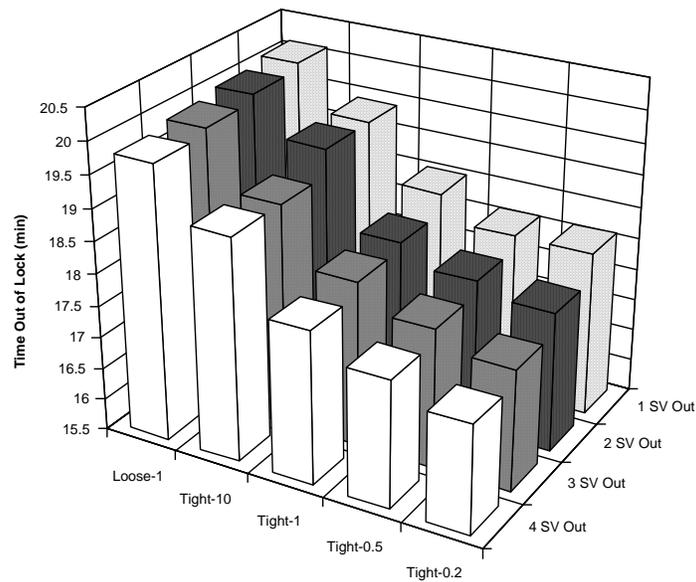The blackout period as a function of IMU architecture and IMU quality is shown in Figure 6.

Figure 6: GPS loss of lock as a function of IMU architecture and quality.

(Note the vertical scale does not begin at zero. The difference is not so striking, as the graph seems to indicate.) For this particular scenario, the performance difference is due to better calibration of the inertial instruments rather than jamming resistance. Even for the best IMU, the blackout time is reduced by only about 2 min from the 20-min blackout experienced by the loosely coupled receiver with full (unaided) bandwidth. Once again, it is difficult to generalize from these results.

For this jammer flyby scenario, the horizontal position errors (root-sum-squared (rss) 1σ) just prior to reacquisition are shown in Figure 7.
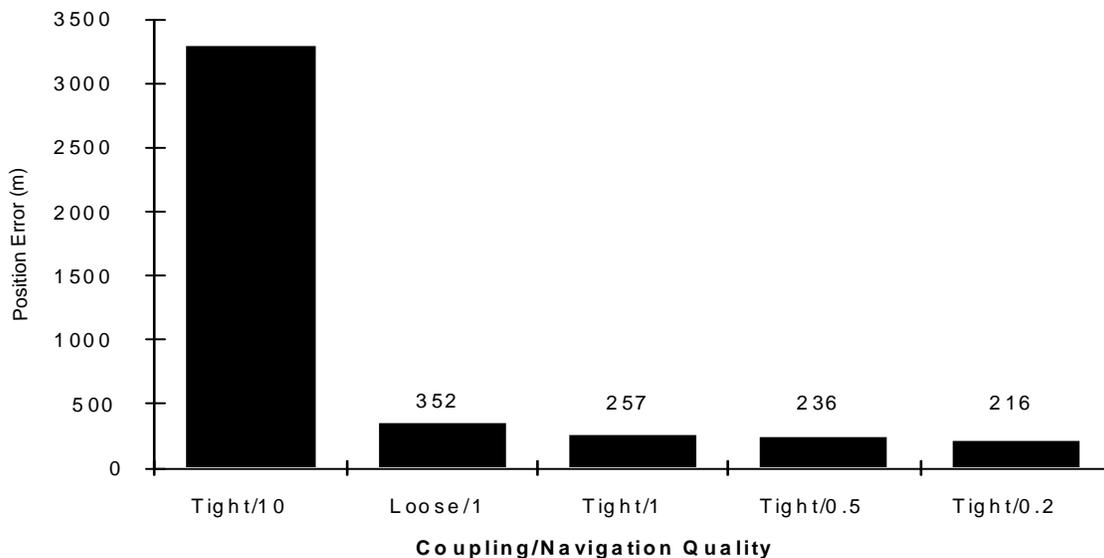
Figure 7: Horizontal position errors just prior to reacquisition.

The ratio of error level between the 10-nmi/h and the 1-nmi/h tightly coupled systems (3300:260) is greater than the 10 to 1 ratio implied by their characterization. Noise is a big error source in the 10-nmi/h system and cannot be calibrated by the GPS measurements as can biases and scale-factor errors. Thus, the better IMUs perform better yet when they are calibrated continuously by in-flight GPS measurements. The tightly coupled 1-nm/h system benefits somewhat more by the GPS in-flight calibration than the loosely coupled system.

2.6.3 Head-on Approach to Jammer

This scenario is meant to simulate the navigation performance of a fighter-bomber mission in which there is a jammer at the target. After take-off, the aircraft climbs to 40,000 ft, dodges a surface-to-air missile, then dives down to 200 ft to get below radar detection and to avoid GPS jamming. On approaching the target area, the aircraft then climbs to a few thousand feet to locate the target, then releases the bomb. The jammer at the target overwhelms all variations of IMU quality and architecture as soon as the aircraft climbs above its horizon. The time interval between loss of lock and bomb release is about 159 s for the loosely coupled system and 153 s for the tightly coupled systems. Figure 8 shows the position error at bomb release for the five navigation systems.
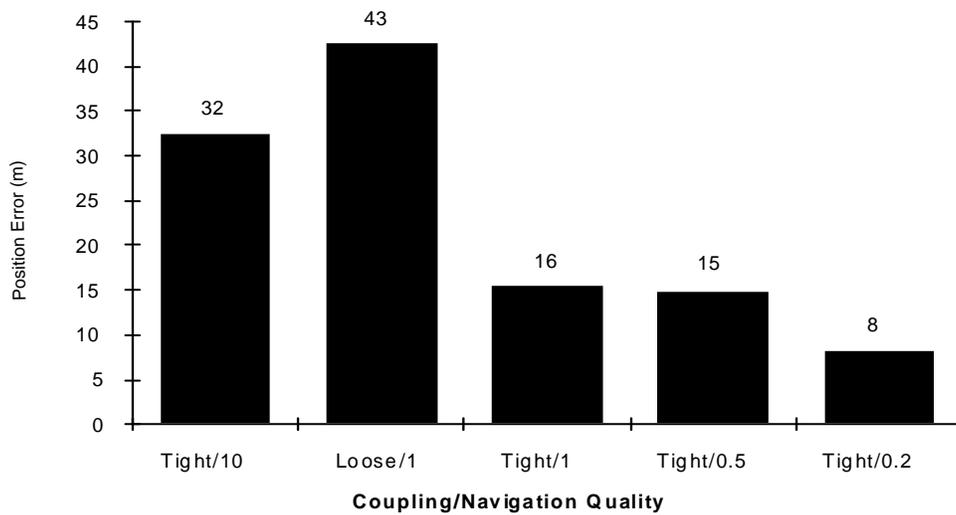

Figure 8: Position errors at bomb release after about 2.7 min of free inertial navigation.

In contrast to the previous scenarios, the IMU performance shortly after loss of lock is shown here. The tightly coupled 10 nmi/h system has better performance than this particular loosely coupled system when GPS measurements are available. After this short a time, 2.7 min, this advantage has not yet been lost. Another contributor to the difference is that the tightly coupled systems resisted the jamming for about 6 s longer than did the loosely coupled system.

2.6.4 Helicopter Performance in Jammer Vicinity

This scenario is meant to depict a helicopter on a scouting mission. The helicopter closely follows the terrain in order to avoid detection. The resulting flight profile has high levels of acceleration and jerk, which caused occasional momentary loss of carrier lock. No effect on mission performance can be seen.

The jamming scenario was simplified for this mission. GPS measurements were available until on-board estimates of IMU calibration and alignment had reached steady state. At that point, GPS was assumed to be jammed. The mission continued for another 19 min. In a variation from the previous scenarios, the navigation system of the helicopter was augmented with ground speed Doppler measurements. These Doppler measurements yield velocity in body coordinates. It will be seen that these measurements make a considerable difference in navigation performance after GPS is lost. The error model for the Doppler measurements is given in Table 8.

Table 8: Error Model for Doppler Ground Speed Measurements.

Error Source	Vertical (1σ)	Horizontal (1σ) (two components)
Bias	0.05 nmi/h	0.1 nmi/h
Scale factor	0.1%	0.25%
Misalignment	2.0 mrad	2.0 mrad

At the end of the mission, the task of the helicopter is to define coordinates of a target at some distance (8 km) from its own position. The error in target coordinates, δr_{tgt}, is thus due to a combination of helicopter location error, $\delta r_{helicopter}$, and IMU misalignment, $\delta\alpha$.

$$\delta r_{tgt} = \delta r_{helicopter} + \delta\alpha \times r$$

where r is the vector from helicopter to target.

Figure 9 shows the error in helicopter position and target location as a function of two IMU qualities when no ground-speed Doppler measurements are included in the navigation solution.
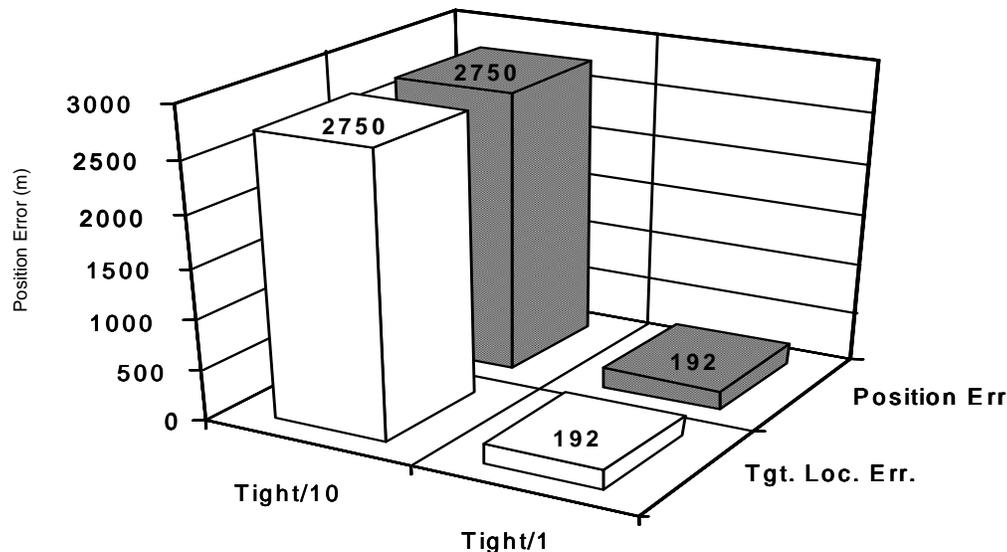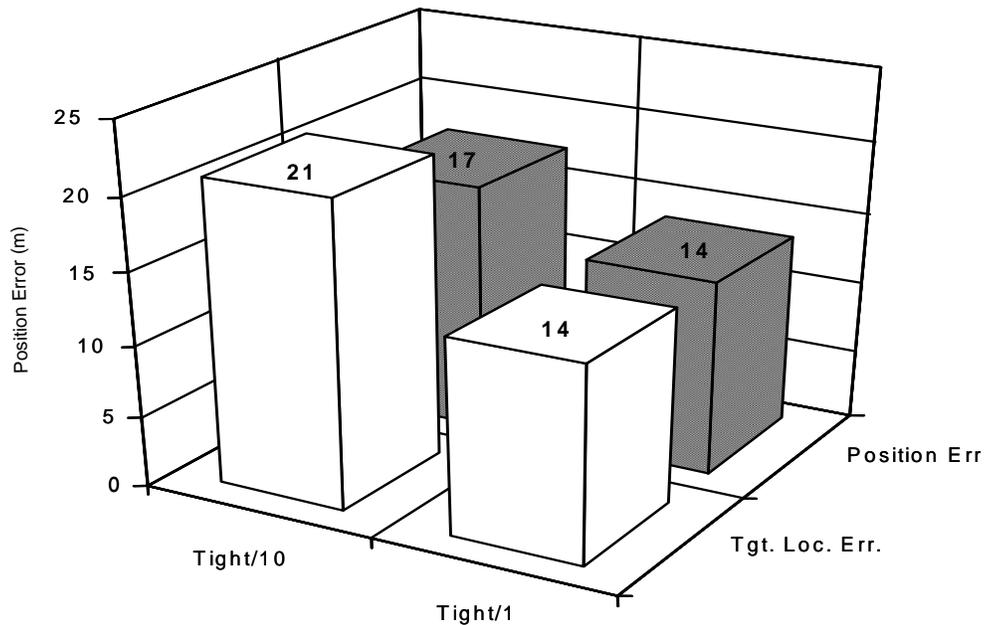

Figure 9: Position and target location errors for a helicopter 19 min after GPS loss of lock without the aid of Doppler ground-speed measurements.

As seen in an earlier scenario, the ratio of the errors between the 10 nmi/h and the 1 nmi/h navigation system, 2750:192 in this case, is greater than the characterization ratio, 10:1. The pointing error is negligible compared with the position error so that the target location errors and the aircraft position errors are essentially the same.

Figure 10 shows the same errors when the navigation solution is aided with ground-speed Doppler measurements. Results for both an INS/GPS system and for an INS/GPS system supplemented with Doppler ground-speed measurements are shown.

**Figure 10: Position and target location errors for scout helicopter 19 min after
GPS loss of lock with the aid of Doppler ground-speed measurements.**

As expected, the Doppler ground-speed measurements slow the error growth that is seen with the free inertial system. These errors in these velocity measurements integrate into growing position errors so they are not equivalent to GPS, which provides position as well as velocity. But they provide much better results than the inertial instruments whose measurements must be integrated twice before yielding position. The improvement with the Doppler ground-speed sensor is dramatic. Note that when aided by these measurements, the performance of the 10-nmi/h system is nearly the same (50% greater target location errors) as that of the 1-nmi/h system.

2.8   Summary of Comparison Results – Loosely Coupled vs. Tightly Coupled

This comparison has illustrated several features of INS/GPS systems that are true in many cases, but there is some danger in drawing general conclusions because the flight profiles and jamming scenarios are quite specific. A particular flight profile may allow more or less in-flight calibration, depending on aircraft maneuvers. These differences can be minimized by including maneuvers whose specific purpose is in-flight calibration and alignment. Jamming scenarios, however, are more difficult to characterize in a general way. Jammers can be on

the ground, in which case, they are shadowed by the terrain for low-altitude approaches. They could also be airborne, in which case, their effective range will be greater, but for which their signal strength will grow with closing distance uncomplicated by shadowing considerations. Furthermore, there may be focused jammers and as a countermeasure to jamming, receiver antennas whose gain can be made a function of direction. All these variables make it difficult to generalize about how much longer a tightly coupled system will be able to maintain lock on the GPS signals. Perhaps the most general statement that can be made is to state the improvement in decibels in signal-to-noise (jammer) ratio that inertially aided receivers achieve.

The in-flight calibration and alignment of the tightly and loosely coupled receivers is simpler to assess. As in this study, loosely and tightly coupled architectures can be proposed. The resulting performance after loss of lock can then be assessed by either Monte Carlo techniques or, as in this study, by linearized covariance analysis.

After doing the analysis and observing simulation results, the following cautious assertions can be made:

1) When GPS is available, its measurements dominate navigation performance. The steady-state navigation error will be reduced by inertial aiding, which simply considered, allows GPS measurement noise to be "averaged out." Improvement of steady-state error with improving inertial quality is not as dramatic.

2) Tight coupling is superior to loose coupling for maintaining lock in a jamming environment, but the gain is hard to quantify, except by improvement in the signal-to-noise (jammer) ratio.

3) Better inertial instruments gain more from in-flight alignment and perform better after GPS is lost. This is because poorer instruments in general have larger proportions of uncalibratable noise.

4) For short time intervals after GPS loss, coupling architectures can make a difference in performance (because they affect calibration and alignment quality).

5) In the long run, basic IMU quality will dominate navigation accuracy due to instrument noise and loss of calibration accuracy.

Finally, it was shown that there is a dramatic difference in jammed performance if Doppler ground-speed measurements were available.

3.0 DEEP INTEGRATION VS. TIGHTLY COUPLED PERFORMANCE COMPARISON[1]

The inertial sensor error model used was representative of a particular Microelectromechanical System (MEMS) IMU capability. Rms accelerometer errors were characterized by 1-mg bias stability, 100-ppm scale-factor stability and 1-cm/s/$\sqrt{h}$ random walk. Rms gyro errors were 10-deg/h bias stability and 0.03-deg/$\sqrt{h}$ random walk. All stability errors were modeled as first-order Markov processes with a time constant of 5 min, which is representative of expected in-flight error characteristics. Accelerometer and gyro input axis nonorthogonalities of 1 mrad, rms were assumed and were treated as fixed biases.

A full 6-degree-of-freedom simulation was used with four satellites continuously in view. The navigation state vector consisted of 3 components of position, velocity, inertial sensor stability errors (bias, scale factor, and misalignment for both accelerometers and gyros), user clock, and clock rate. Clock errors were treated as biases. Satellite ephemeris errors were accounted for by including an unestimated range bias of two meters, rms.

---

[1] The material in this section is from References 3 and 4. "Deep integration" is trademarked by Draper Laboratory.

The navigation algorithms are nonlinear. Thus, it was not possible to perform an accurate error covariance analysis based on linearization. As a consequence, the results in this section are based on Monte Carlo analysis.

The measurements from all correlators were processed simultaneously, while the measurements from each satellite were processed sequentially. An ideal correlation function was assumed in the navigation algorithms, with $R_c(\tau) = 1 - |\tau|$ for $|\tau| \leq 1$ and $R_c(\tau) = 0$ for $|\tau| > 1$. A correlator spacing of ½ chip was used throughout. Two types of jammers were assumed: 1) wideband Gaussian jammer with a 20 MHz bandwidth, and 2) narrowband jammer with a 1 kHz bandwidth. Jammer outputs were generated using a first-order Markov process driven by pseudorandom Gaussian noise.

In order to assess performance relative to conventional systems, a tightly coupled INS/GPS system was also simulated. The simulation model assumed a GPS receiver capable of calculating pseudo-range and delta-range. The receiver outputs and the simulated MEMS sensor outputs were fed to an INS/GPS integration filter. This filter was mechanized as a standard extended Kalman filter and used the same navigation state vector as the deeply integrated system. The receiver was velocity aided using the velocity components of the state vector estimate. The tightly coupled receiver filter bandwidth was 0.1 Hz while in State 3 tracking. Code loop loss-of-lock was assumed to occur at J/S = 54 dB. Above this threshold, GPS data were not used and free inertial navigation was assumed.

3.1   Constant Wide-Band Gaussian Jamming

Performance comparisons between the deeply integrated and tightly coupled systems were first conducted for two scenarios in which the navigator is subject to a constant wide-band Gaussian jamming. This allows the assessment of the additional loss-of-lock capability due to deep integration in a relatively straightforward manner. Dynamic maneuvers were simulated: body-frame specific force was pulsed between 0 and ±1 g along all axes; pulsewidth was 10 s with a period of 90 s.

Results for the first scenario are shown in Figure 11 using 27 Monte Carlo runs. J/S was maintained at 30 dB over the first 60 s of flight and then instantaneously switched to a higher value and held there for the remainder of the 5-min flight. Initial rms navigation errors were 30 m and 1 m/s along each axis. Initial rms clock errors were 20 m and 2 m/s. J/S levels used were 40 to 80 dB in increments of 5 dB, as shown outside the right edge of the figures. The deeply integrated system was able to maintain code lock up to 65 dB J/S, an improvement of approximately 15 dB over the tightly coupled system. Note also that the deeply integrated system achieves lower rss error during the 60-s initialization phase.
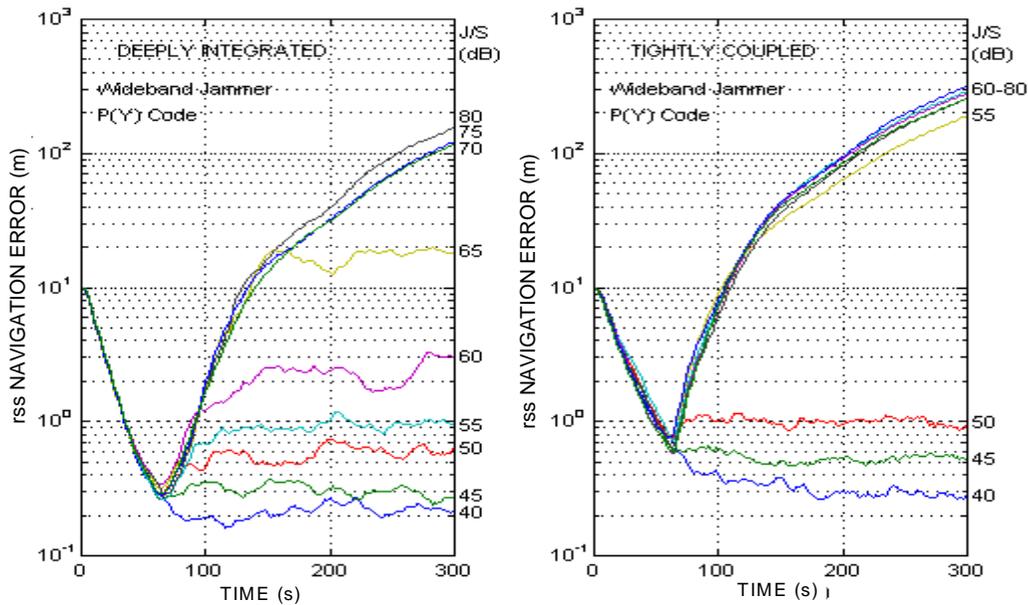
Figure 11: Navigation performance comparison: first scenario.

The second scenario used a constant value of J/S over a 7-min flight. Initial rms position and velocity errors were 2 m and 1 m/s along all axes. The rms clock errors were 1 m and 0.1 m/s. J/S was varied between 50 and 80 dB in 5-dB increments. The results are shown in Figure 12, using 35 Monte Carlo runs and for both 10-deg/h and 1-deg/h INS error models. The results again indicate a significant improvement in loss-of-lock capability due to deep integration. This improvement is shown quantitatively in Figure 13, in which the results of Figure 12 are replotted vs. antijam (A/J) improvement. A/J improvement is in excess of 10 dB at all values of rss error and exceeds 15 dB for rss error greater than 35 m. Note that the A/J improvement also increases when higher quality inertial sensors are employed. This is primarily due to the enhanced in-flight error calibration capability of the deeply integrated system.
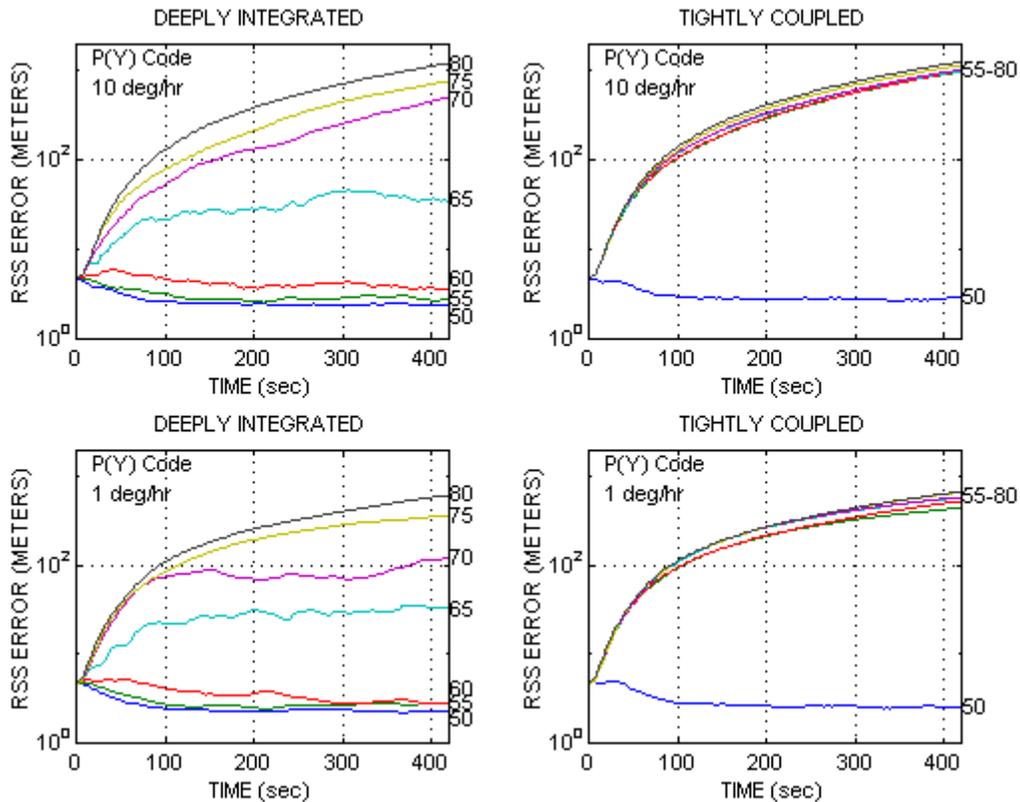
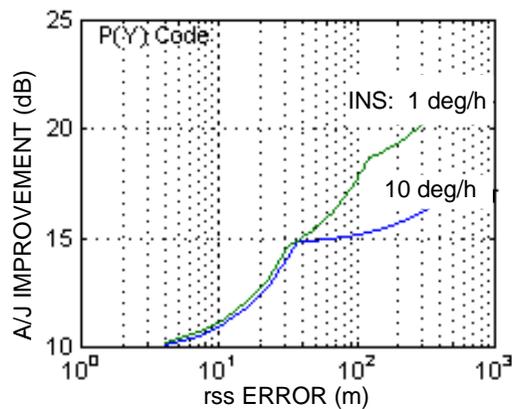**Figure 12: Navigation performance comparison: second scenario.**

Figure 13: A/J improvement due to deep integration.

3.2   Precision Guided Munition Scenario

The performance of the deeply integrated navigation system was evaluated for a precision guided munition (PGM) scenario in which the target was at a range of 63 nmi. The altitude profile is plotted in Figure 14. A single wideband Gaussian jammer was placed 5 nmi in front of the target in an attempt to simulate a worst-

case scenario for a single jammer. This placement gives maximum J/S prior to final target approach with a resultant loss of navigation system performance just prior to target impact. The J/S history for a 100 W jammer is shown in Figure 15.
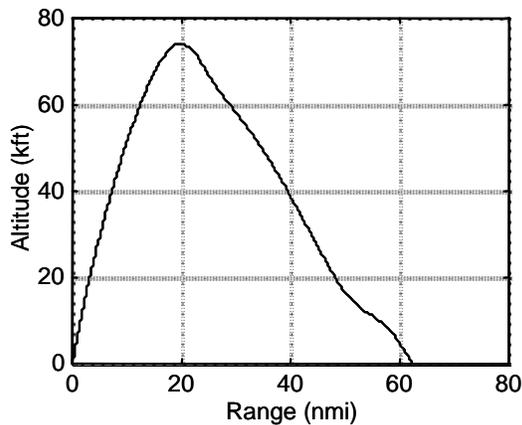

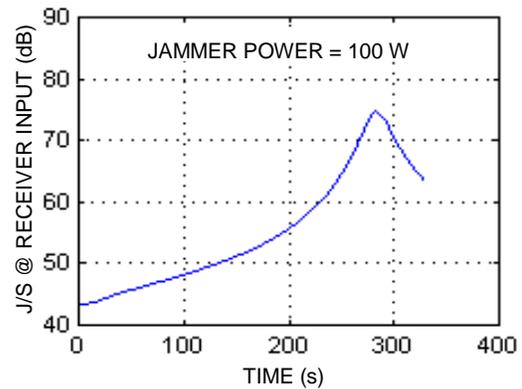Figure 14: PGM altitude profile.

Figure 15: PGM scenario: J/S vs. time.

Performance was evaluated by varying the jammer power from 1 W to 10 kW. A total of 25 Monte Carlo runs was made at each power level. Initial rms navigation errors were 10 m and 0.2 m/s per axis; initial rms clock errors were 10 m and 0.2 m/s. The CEP at target impact is plotted vs. jammer power for wideband jamming in Figure 16 and for narrowband jamming in Figure 17. Comparing the results in the figures, it can be seen that the deeply integrated system offers significant improvement over the traditional tightly coupled system for both wideband and narrowband jamming. As an example, a 100-W wideband jammer results in a CEP of 11 m for the deeply integrated system, compared with a CEP of 120 m for the tightly coupled system. If the jammer power is reduced to 10 W, the CEP values are 2.6 m for the deeply integrated system and 71 m for the tightly coupled system.
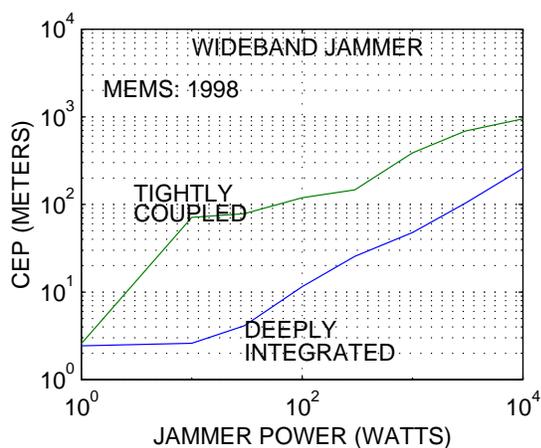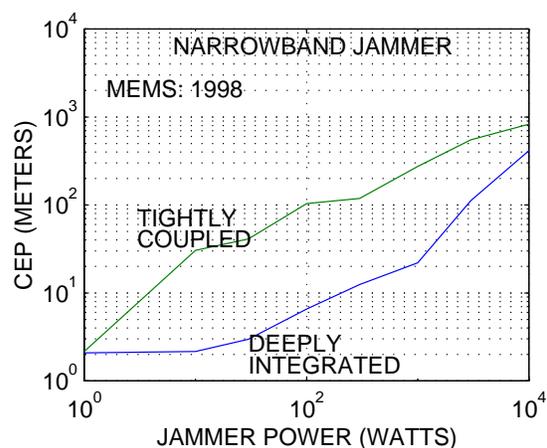

Figure 16: CEP vs. jammer power: wideband jammer.

Figure 17: CEP vs. jammer power: narrowband jammer.

A/J improvement capability may be quantified by comparing jammer power at a constant value of CEP. The resulting improvement in A/J capability due to deep integration can be seen in Figure 18. For wideband jamming, improvements of at least 15 dB are seen for CEP values ranging from 6 to 120 m. For narrowband jamming, improvements of at least 15 dB are seen for CEP values ranging from 4 to 80 m. Improvement is seen to decrease as the CEP decreases below 10 m. In this case, the decrease in CEP results from a decrease in jammer power, and the tightly coupled system tends to maintain lock with higher probability as the jammer power decreases. In the limit as the jammer power approaches zero, the tightly coupled system approaches efficient operation, and both systems give comparable performance. The improvement is also seen to decrease as the CEP increases beyond 100 m. In this case, the increase in CEP results from an increase in jammer power and the tracking quality of the deeply integrated system begins to degrade. In the limit as the jammer power increases without bound, the deeply integrated system can no longer maintain lock, and both systems are operating in a free inertial mode where the CEP is determined solely by initial navigation errors and inertial sensor errors.
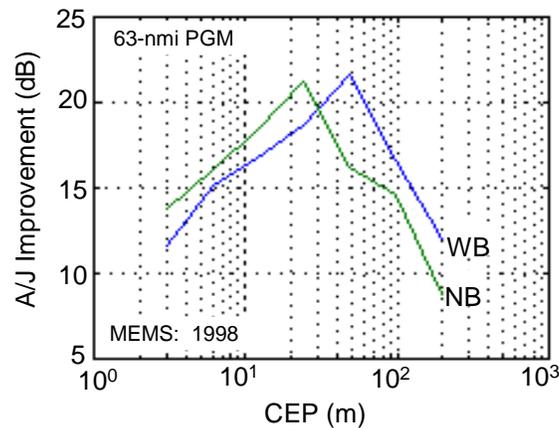

Figure 18: A/J improvement due to deep integration.

3.3   Final Comment on Deep Integration Comparison

As shown in Reference 5, every 20 dB increase in A/J improvement in the INS/GPS system requires that the jammer increase its power by a factor of 100 to maintain the same effectiveness as a jammer. Yet the increase in jammer power makes its detection and attack much more probable. Thus, the potential benefits of deep integration are substantial in both comparisons reported here. Additional comparisons can be found in Gustafson and Dowdle, "Deeply Integrated Code Tracking," ION GPS/GNSS Portland, OR, 2003.

4.0   CONCLUDING REMARKS

This paper has presented several options for the integration of INS and GPS systems in order to benefit from the advantages of each system. As been shown, if the integration level between the two systems increases, the benefits also generally increase. The comparison of deeply integrated vs. closely coupled indicates that the deeply integrated approach will likely find more applications in the future.

REFERENCES

[1] Schmidt, G. and Phillips, R., *INS/GPS Integration Architectures*, NATO RTO Lecture Series, RTO-EN-SET-116, *Low-Cost Navigation Sensors and Integration Technology*, March 2011.

[2] Johnson, Gregory B., Lewantowicz, Zdzislaw H. "Closed Loop Operation of GPS Aided INS," *Third International Technical Meeting of the Satellite Division of the Institute of Navigation Proceedings*, The Institute of Navigation, Washington, D.C., pp. 461-470, 1990.

[3] Gustafson, D. et al., *A Deeply Integrated Adaptive GPS-Based Navigator with Extended Range Code Tracking,* Draper Laboratory Report P-3791, Cambridge, MA, January 2000. Also, IEEE PLANS Conference, San Diego, CA, March 2000.

[4] Gustafson, D. et al., *A High Antijam GPS-Based Navigator*, Draper Laboratory Report P-3776, Cambridge, MA, January 2000. Also, Institute of Navigation National Technical Meeting, Anaheim, CA, 2000.

[5] Schmidt, G., *INS/GPS Technology Trends*, NATO RTO Lecture Series, RTO-EN-SET-116, *Low-Cost Navigation Sensors and Integration Technology*, March 2011.